Part I

THE THEORETICAL PROBLEM

Chapter 2. A Ray Approximation Theory for Multiple Modelling and Suppression

In this chapter we intend to solve the slanted forward and inverse problems within the scope of the Noah approximation as defined by Riley [17]. That is, for a two-dimensional layered earth, where diffractions, transmission effects and intrabed multiples are absent. The terms "forward" and "inverse" seem to derive from the fact that reflection seismology can be considered as a filter problem, with the input being the signal from some acoustic source at or near the earth's surface. The filter is the earth itself and the output, the recorded seismogram (Figure 2.1). Denoting B to be the input signal, E to be the impulse response of the earth and R the recorded seismogram, we can identify two major problems, which are: 1) the forward problem, given B and E, find R; and 2) the inverse problem, given B and R, find E. In terms of multiple reflections, the forward problem allows their modelling, while the inverse, their suppression. However, we will discuss the problem as a wave propagation phenomenon.

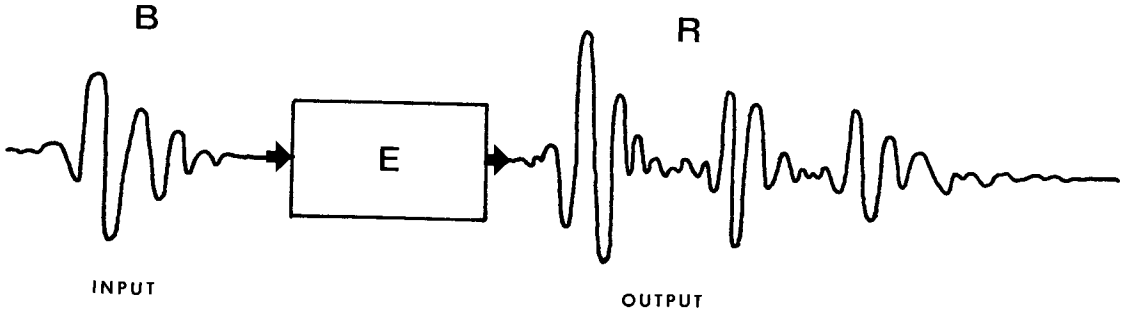

Figure 2.1. Reflection seismology as a filtering process. If we call E the earth's impulse response, then given the shot waveform B, the reflection seismogram R can be computed as $R = E * B$, where "$*$" denotes convolution.

Before considering the forward and inverse problems, we need to do a few preliminary steps. First we need to define the appropriate coordinate systems to express our variables and equations. Under the assumption of a two-dimensional earth we will be dealing, mainly, with three coordinates (Figure 2.2a): the horizontal or offset coordinate (x) , the vertical or depth coordinate (z) , and the travel time (t) . The separation of the wave field into two different components, up (U) and downgoing (D) waves, that propagate in opposite directions, further suggests the introduction of separate coordinate frames for each one of them. In particular, it is convenient to associate a coordinate axis with the direction of propagation of each wave. The situation is illustrated in Figure 2.2b, where a coordinate frame corresponding to a downgoing plane wave that propagates from left to right an an angle θ is depicted. The frame for the upcoming wave is shown in Figure 2.2c. We will associate the coordinates (x, z, t) with the observer frame, (x", z", t") with the downgoing waves (D) and (x', z', t') with the upcoming waves (U) .

Furthermore, in order to implement computer algorithms, we will define a set of discrete coordinates (j, k, n) according to:

$$x = j\,Dx \;;\quad z = k\,Dz \quad \text{and} \quad t = n\,Dt \;, \tag{2-1}$$

where, Dx, Dz and Dt are the sampling intervals along x , z and t respectively. In this notation, U(x,z,t) then refers to function U defined in a continuum, while $U^n_{k,j}$ is the same function in the corresponding discrete space. Figure 2.3 indicates that, once Dx and θ have been defined, a suitable choice for Dz and Dt could be :

$$Dz = Dx/\tan(\theta) \qquad (2\text{-}2a)$$

$$Dt = Dx / (v \sin(\theta)) \ . \qquad (2\text{-}2b)$$

The second parameter we have to define in our general problem is the propagating medium, that is, the earth model. In this respect one of the simplest models that can be considered is that of a horizontally stratified earth (one-dimensional model). This model requires all the medium's characteristics (reflection $c(z)$ and transmission $t(z)$ coefficients, velocities $v(z)$, etc.) to be functions of depth only, which from now on we will associate with the coordinate z . In many cases an additional simplification is introduced: the elastic parameters vary in such a way that velocity is expected to remain constant. In our study we will be using a two-dimensional model. Our medium will allow for depth and lateral variations of the reflectivity and other elastic constants. The lateral variations, though, will be considered small enough as to be able to ignore back scattered waves. For computational and illustrative reasons the medium may be divided into horizontal slices, but the layers need not be horizontal. Finally, although not a necessary condition, for simplicity most of the time we will ignore transmission effects and intrabed multiple reflections. These approximations seem pretty reasonable in quite a large number of real data examples and, especially, in marine seismograms. In the cases where it is not true, the inclusion of transmission coefficients and intrabed multiples do not represent a major problem.

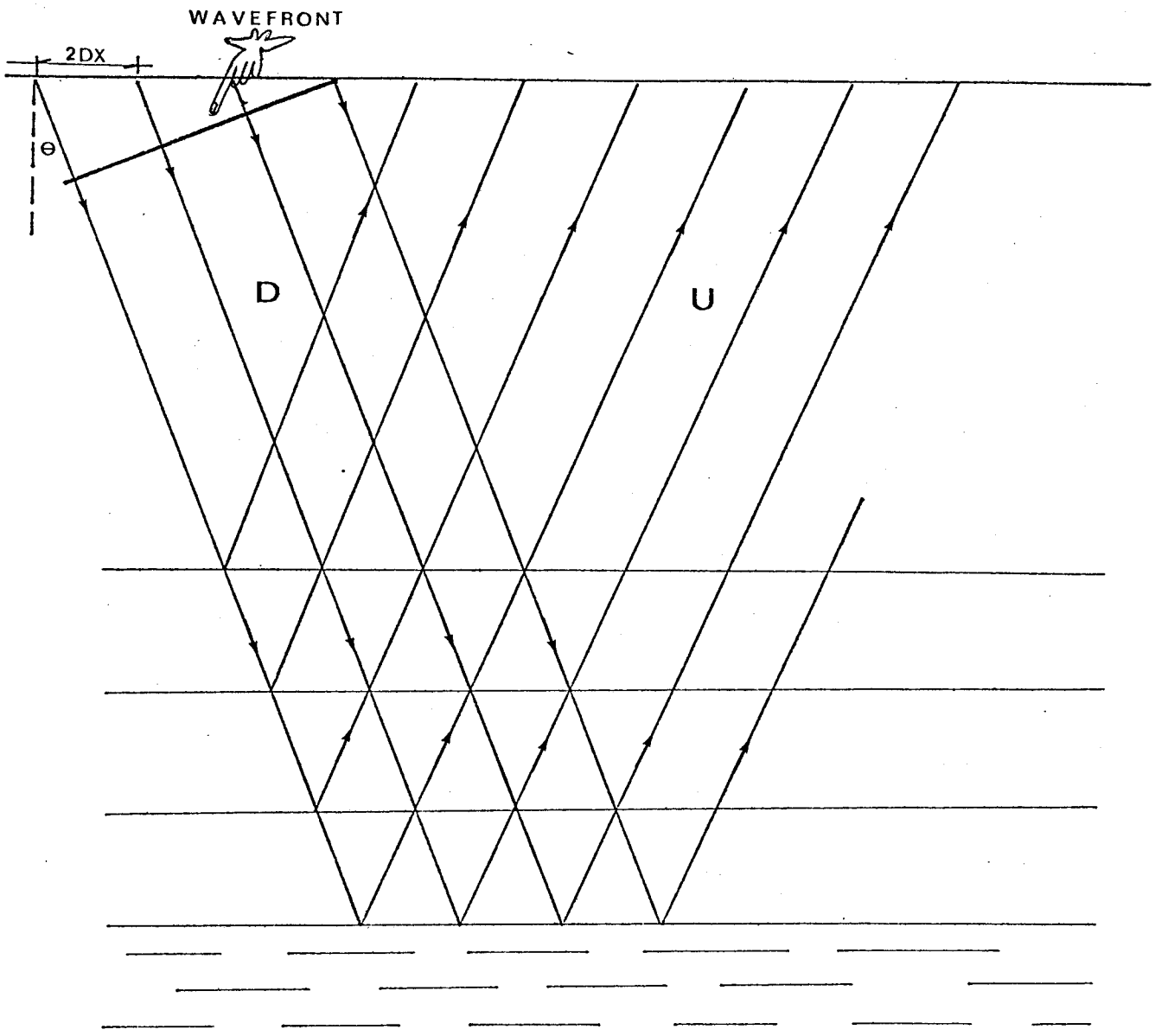

Figure 2.3. Slanted propagation in layered media. The ray diagram for a plane wave that propagates from left to right at an angle θ to the vertical is shown in this figure. We assume that both shots and geophones have the same separation, 2 Dx .

Finally, we need an operator which is capable of propagating the wave fields through the acoustic media. Here we have several choices. The most simple one is to assume a ray approximation for the wave propagation, in which case the energy will be merely translated from point to point along ray paths ([3], [12], [14]). Although this model allows for variations of the reflectivity and velocity along the wave trajectories, it excludes diffractions. If we want to include diffractions in our analysis, then we can make use of the more general differential equations that describe the propagation of acoustic or elastic waves ([5], [15]). Expressed through finite difference or finite element approximations, these equations may be used as wave propagators. We could also use an integral solution to the wave equation, e.g. Kirchhoff Integral ([13], [11]), as a means for propagating the wave fields. In our analysis, however, we will follow only the first two options, since the last one seems to be troublesome when considering variable velocity media. Moreover, we will limit our present study to the use of the two-dimensional scalar acoustic wave equation.

2.1. Noah Slanted Deconvolution

Despite its limitations, a ray propagation-layered medium approximation has proven to model many important real data cases reasonably well. The fact that the earth itself tends to be horizontally layered and that diffractions are only noticed in relation to very disturbed geological interfaces may account for this. On the other

For most cases we can neglect transmission effects and intrabed multiples, which is equivalent to assuming $\bar{t} \cong \underline{t} \cong 1$ and $\underline{c} \cong 0$ respectively. Thus, equations (2-3) become:

$$\bar{U} \cong \underline{U} + \bar{c}\,\bar{D} \tag{2-4a}$$

$$\underline{D} \cong \bar{D} \tag{2-4b}$$

If now we discretize U and D according to (2-1), equations (2-4) can be rewritten as:

$$\bar{U}^{n'}_{k',j'} \cong \underline{U}^{n'}_{k',j'} + \bar{c}_{k',j'}\,\bar{D}^{n''}_{k'',j''} \tag{2-5a}$$

$$\underline{D}^{n''}_{k'',j''} \cong \bar{D}^{n''}_{k'',j''} \tag{2-5b}$$

For reasons that will be obvious shortly, it is convenient to express U and D as lower-bar variables only. Noticing that within each layer the waves do not change, we can write $\bar{U}^{n'}_{k',j'} = \underline{U}^{n'+1}_{k'-1,j'}$ and $\bar{D}^{n''}_{k'',j''} = \underline{D}^{n''-1}_{k''-1,j''}$. Replacing in (2-5) we get:

$$\underline{U}^{n'+1}_{k'-1,j'} = \underline{U}^{n'}_{k',j'} + \bar{c}_{k',j'}\,\underline{D}^{n''-1}_{k''-1,j''} \tag{2-6a}$$

$$\underline{D}^{n''}_{k'',j''} = \underline{D}^{n''-1}_{k''-1,j''} = \ldots = \underline{D}^{n''-k''}_{0,j''} \tag{2-6b}$$

Hereafter, U and D will always refer to the "lower-bar" variables of each interface ($U = \underline{U}$, $D = \underline{D}$) and c to the "upper" ones ($c = \bar{c}$) . Besides, to be consistent, we have to express all variables in equation (2-6a) as functions of a unique coordinate system. An examination of Figures 2.2 and 2.3 shows that $D^{n''-k''}_{0,j''} = D^{n'-k'}_{0,j'-k'}$. Making this substitution into (2-6a) and dropping primes we obtain:

$$U^{n}_{k,j} = U^{n-1}_{k+1,j} + c_{k+1,j}\, D^{n-k-1}_{0,j-k-1} \qquad (2\text{-}7a)$$

This difference equation allows us to extrapolate upcoming waves from within the earth up to the surface. If we want to bring them from the surface back into the earth, then equation (2-7a) can be re-expressed as:

$$U^{n}_{k,j} = U^{n+1}_{k-1,j} - c_{k,j}\, D^{n-k}_{0,j-k} \qquad (2\text{-}7b)$$

Equations (2-7) are supplemented by several boundary and initial conditions:

1) The upcoming wave at the surface is the reflection seismogram R^{n}_{j} :

$$U^{n}_{0,j} = R^{n}_{j} \qquad (2\text{-}8)$$

2) We will assume that the upper boundary of the medium (air-water interface in the case of marine data) is a perfect reflector ($\underline{c} = -1$). Thus, according to Figure 2-5:

3) Causality tells us that at a given boundary we cannot have an upcoming wave before a downgoing wave encounters the interface. Mathematically this means that:

$$\underline{U}^{n}_{k,j} = \bar{U}^{n-1}_{k+1,j} = 0 \quad \text{for} \quad n \leq k \; . \tag{2-11}$$

An important consequence of the above is that by making $n = k$ in expression (2-10b) and according to (2-11) we have:

$$U^{k+1}_{k-1,j} = c_{k,j} \, D^{0}_{0,j-k} = c_{k,j} \, (\, B^{0}_{j-k} - R^{0}_{j-k} \,)$$

or

$$c_{k,j} = U^{k+1}_{k-1,j} \; / \; B^{0}_{j-k} = \bar{U}^{k}_{k,j} \; / \; B^{0}_{j-k} \tag{2-12}$$

Equations (2-7) plus the additional boundaries and initial conditions (2-8) through (2-11) define a well-posed problem, perfectly suitable for solving either the forward or inverse problem. Given the shot waveform B and the reflection coefficients $c(x,z)$, in order to solve the forward problem we start with $U^{k+1}_{k-1,j} = B^{0}_{j-k} \, c_{k,j}$ and use equation (2-7a) to extrapolate this upcoming wave up to the surface. If given instead R and B, we start with $U^{n}_{0,j} = R^{n}_{j}$ and use equation (2-7b) to bring this wave back down into the earth, till we get $U^{k+1}_{k-1,j}$. Then (2-12) allows us to compute the reflection coefficients. We actually can reproduce this recursion in order to obtain a more compact and familiar expression. In effect, for the forward problem we have that

$$R_j^n = U_{0,j}^n = U_{1,j}^{n-1} + c_{1,j}\, D_{0,j-1}^{n-1} = U_{2,j}^{n-2} + c_{2,j}\, D_{0,j-2}^{n-2} + \tag{2-13}$$

$$+ c_{1,j}\, D_{0,j-1}^{n-1} = \ldots = U_{n/2-1,j}^{n/2+1} + \sum_{i=1}^{n/2-1} c_{i,j}\, D_{0,j-i}^{n-i}$$

Renaming indexes, this relation can be re-expressed as:

$$R_j^{2n} = B_{j-n}^0\, c_{n,j} + \sum_{i=1}^{n-1} c_{i,j}\, (B_{j-i}^{2n-i} - R_{j-i}^{2n-i}) . \tag{2-14}$$

The "2n" in B and R is because we defined Dt as the one way travel time between layers $Dt = Dx / (v\sin(\theta))$. Actually it is more convenient to define it as the two way travel time $Dt = 2\, Dx / (v \sin(\theta))$. This implies sampling B and R in time half as often as before. With this convention we then can re-write (2-14) as:

$$R_j^n = B_{j-n}^0\, c_{n,j} + \sum_{i=1}^{n-1} c_{i,j}\, (B_{j-i}^{n-i} - R_{j-i}^{n-i}) . \tag{2-15}$$

Correspondingly, for the inverse problem we can start from:

$$B_{j-k}^0\, c_{k,j} = U_{k-1,j}^{k+1} = U_{k-2,j}^{k+2} - c_{k-1,j}\, D_{0,j-k+1}^1 = \ldots , \tag{2-16}$$

which, after the same considerations as before, produces:

$$c_{k,j} = (R_j^k / B_{j-k}^0) - (1 / B_{j-k}^0) \sum_{i=1}^{k-1} c_{i,j}\, (B_{j-i}^{k-i} - R_{j-i}^{k-i}) . \tag{2-17}$$

If we assume that the shot waveform is just a single pulse ($B_j^n = B_j^0 = 1$), then (2-15) and (2-17) simplify into:

$$R_j^n = c_{n,j} - \sum_{i=1}^{n-1} c_{i,j} R_{j-i}^{n-i} \qquad (2\text{-}18)$$

and

$$c_{k,j} = R_j^k + \sum_{i=1}^{k-1} c_{i,j} R_{j-i}^{k-i} \quad . \qquad (2\text{-}19)$$

Since we are assuming an impulsive shot waveform, in the two last relations R refers to the "white" seismogram (shot waveform removed). In contrast, the R of expressions (2-15) and (2-17), is rather the actual recorded or "colored" seismogram (shot waveform included). Expressions (2-15) through (2-19) are very similar to those obtained by Riley in his one-dimensional algorithm and, for the case of vertical propagation, they actually become identical.

Expressions (2-18) and (2-19), which imply feed-back recursions are numerically stable. The situation with (2-15) and (2-17) is somehow different since stability here requires the shot waveform to be minimum phase, especially when solving the inverse problem. Hence, for the practical implementation of the algorithm we have two alteratives: 1) either we use the recorded seismogram R and apply (2-17) under the assumption that the estimated input waveform B is minimum phase, or 2) we deconvolve first the recorded seismogram with the estimated waveform B and then use the obtained "whitened" seismogram in conjunction with (2-19). Since in most of the field data cases B tends to be non-minimum phase, the second alternative seems more practical. In any case, whatever alternative we follow, it is important to point out that both options require a good knowledge of the shot waveform B. Some methods for its estimation will be discussed in the last chapter.

Finally, I would like to remark that (2-15) and (2-17) are actually two different representations of the same basic relation, thereby a single computer algorithm can be used to solve both the forward and the inverse problems. Memorywise, the algorithm is very efficient and computations can be greatly reduced by carefully gating the data as to avoid unnecessary calculations. This applies, for instance, to the water layer which in some cases can be significantly large. Detailed gating techniques are discussed by Riley (1976).

2.2. Synthetic Examples

The first example in Figures 2.6 and 2.7 illustrates the amplitude correction that we may expect from a slanted theory, if the reflection coefficients vary laterally. The "earth model" corresponds to a terminating horizontal reflector, overlaying a deeper flat reflector with reflection coefficients c_1 and c_2 respectively. Figure 2.6 indicates that for the first order peg-leg we have to consider two different paths (continuous and dashed lines). Starting with the shots at the extreme right of the figure, each path bounces once from each reflector (Figure 2.6a), arriving at the surface with an amplitude equal to $-c_1 c_2$ (assuming that a unit amplitude impulse was sent into the earth). Since in this case both trajectories reach the surface at the same time, the total recorded amplitude will be $-2 c_1 c_2$. But as the shots move toward the left (Figure 2.6b) one of the two peg-leg reflections is lost (the short-path-last). Thus, this reflection is half the strength of the previous case, that is, $-c_1 c_2$. Similarly, for the second order peg-leg we shall start with three

different paths accounting for a total amplitude of $3\ c_1^2\ c_2$; but after the short-path-last reflection hits the edge of the first reflector, two reflections are lost and, consequently, the amplitude should decay to 1/3 of its initial value. Figures 2.7a, b and c illustrate these considerations. Figure 2.7a shows the model, followed in 2.7b by the computed vertical reflection seismogram (forward problem). As the theory predicts, no lateral variations in amplitude are observed in any of the multiple reflections (M_1, M_2, PL_1, PL_2, etc.). On the other hand, Figure 2.7c shows for a slanted plane wave that propagates from right to left that the amplitudes of the peg-leg reflections (PL_1 and PL_2) do indeed vary laterally according to Figure 2.6.

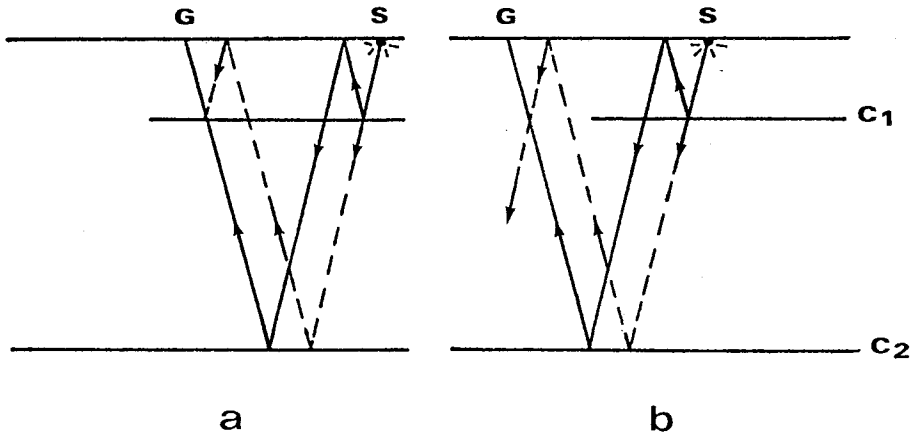

Figure 2.6. First order peg-legs for a terminating horizontal reflector (c_1) . When the sources at the right are sufficiently far from the edge of the first reflector (a), the geophones will record both paths (solid and dashed lines). But as the sources approach the reflector's cut-off, the short-path-last peg-leg is lost and the geophones will record only half the amplitude recorded at the right for the same peg-leg.

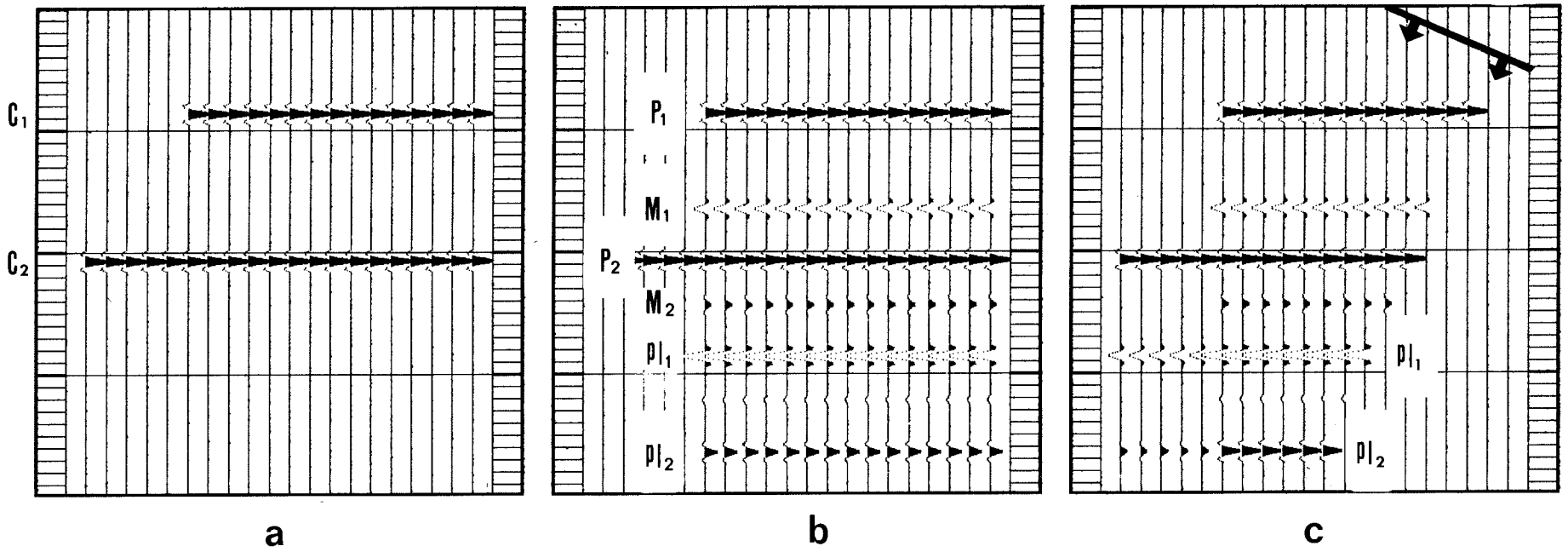

Figure 2.7. Reflection seismograms in the case of a terminating horizontal reflector. Figure (a) shows the initial model, where the surface is considered to be a perfect reflector. (b) is the reflection seismogram corresponding to a wave that propagates vertically downward. P_1 and P_2 are the primary arrivals, M_1 and M_2, the first and second order multiples and PL_1, PL_2, the first and second order peg-legs. Figure (c) shows the seismogram for a wave that travels from right to left as indicated in the upper right corner. Here the peg-leg reflections vary laterally according to Figure 2.6: the amplitude of PL_1 on the left side is 1/2 of its amplitude on the right and the amplitude of PL_2 on the left is 1/3 of its amplitude on the right.

Figures 2.8 and 2.9 illustrate other differences between vertical and slant seismograms. Figure 2.8a shows the model considered, followed in 2.8b by the vertical seismogram and, for comparison, the slant seismogram in 2.8c. As before, $P_1 - P_2$ are the first arrivals, $M_1 - M_2$, the sea bottom multiples and $PL_1 - PL_2$, the corresponding peg-legs.

First, notice that the multiples produced in the two cases (vertical and slant) are different. The difference in arrival times is due to the separate paths followed by the rays in each case, while the difference in shapes is due to the fact that each time the ray reflects from the irregular "sea bottom", it picks up a different structural frequency as shown in Figure 1.2.

Secondly, an interesting effect can be noticed on the peg-legs. Since the travel times involved in this case are longer than in the case of simple multiples, we expect greater differences in shapes as well as in arrival times when considering all the trajectories of a given order. Again the difference in shapes arises from the fact that each kind of peg-leg will reflect a distinct geological frequency. In this case, as shown in Figure 2.9, the short-path-first peg-leg will image low wavelengths, while the remaining will reflect the high wavelengths of the "sea bottom". The travel time separation of the two peg-legs seen in Figure 2.8, is obvious in Figure 2.9, where it is shown that the short-path-first peg-leg (low frequencies) will arrive first.

Finally, Figures 2.10 and 2.11 illustrate the inverse algorithm for the same model of Figure 2.8. Figure 2.10a shows the initial "earth model", (b) the corresponding slanted reflection seismogram and (c) the reconstructed earth model, computed from the reflection seismogram. Figures 2.11 (a) , (b) and (c) repeat the previous sequence but for a model with a relatively large noise level, in order to test the stability of the algorithms in the presence on random background noise. As 2.11b and 2.11c show, the results are quite acceptable.

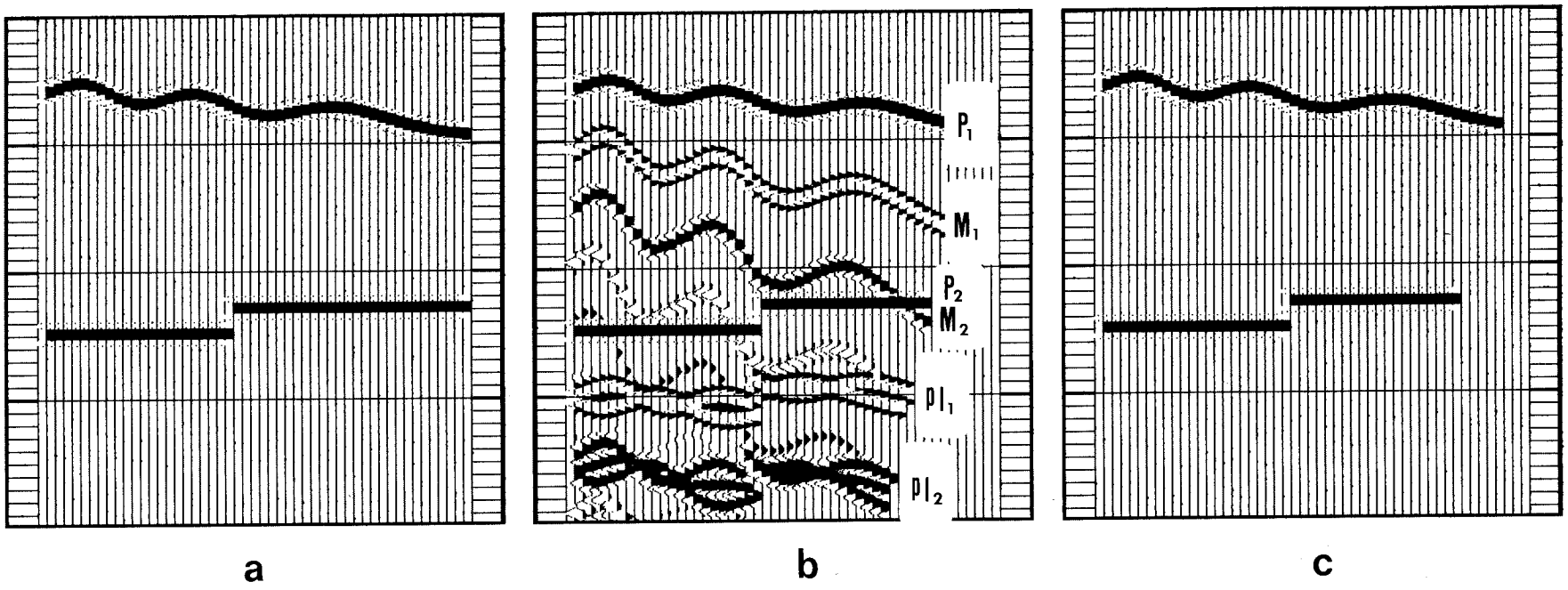

Figure 2.10. Results from the forward and inverse algorithms. (a) shows the initial earth model of Figure 2.9. Figure (b) is the output from the forward algorithm corresponding to the slanted reflection seismogram. (c) is the reconstructed model obtained from the seismogram (b) and the inverse algorithm. In the case of steep dips and/or poor sampling in t , an interpolating scheme may be necessary in order to properly locate and subtract the predicted values.